THE JOURNAL OF PHYSICAL CHEMISTRY C

Article

pubs.acs.org/JPCC

Local Structure of Cationic Sites in Dehydrated Zeolites Inferred from ^{27}Al Magic-Angle Spinning NMR and Density Functional Theory Calculations. A Study on Li-, Na-, and K-Chabazite

Petr Klein,[†,§] Veronika Pashkova,[†] Haunani M. Thomas,[†] Sarah R. Whittleton,[†] Jiri Brus,[‡] Libor Kobera,[‡,∥] Jiri Dedecek,[†] and Stepan Sklenak*[,†]

[†]J. Heyrovsky Institute of Physical Chemistry, Academy of Sciences of the Czech Republic, Dolejškova 3, CZ 182 23 Prague 8, Czech Republic

[‡]Institute of Macromolecular Chemistry, Academy of Sciences of the Czech Republic, Heyrovsky sq. 2, CZ 162 06 Prague 6, Czech Republic

[§]Department of Inorganic Technology, Faculty of Chemical Technology, University of Pardubice, Doubravice 41, Pardubice, CZ 532 10, Czech Republic

ABSTRACT: High-resolution ^{27}Al magic-angle spinning (MAS) NMR spectroscopy of dehydrated M-forms (M = Li, Na, and K) of chabazite in tandem with density functional theory calculations are employed to study the quadrupolar interaction of ^{27}Al nuclei in dehydrated zeolites and to understand the corresponding high-resolution ^{27}Al MAS NMR spectra. We show that the broadening of the ^{27}Al NMR signal in dehydrated zeolites occurs predominantly because of the deformation of the local structure of AlO_4^- tetrahedra caused by the binding of M^+ to the zeolite framework. This deformation increases with the decreasing diameter of the cations from K^+ to Li^+. The influence of water in hydrated zeolites is limited only to prevent a strong coordination of the M^+ cation to O atoms of the AlO_4^- tetrahedron, but there is no "averaging" effect concerning the local electrostatic field due to molecular motion of water molecules. Our results show that the ^{27}Al NMR parameters in dehydrated zeolites can be calculated accurately enough to allow the description of the local structure of AlO_4^- tetrahedra in dehydrated zeolites and to infer the local structure of the sites accommodating the extraframework M^+ cations.

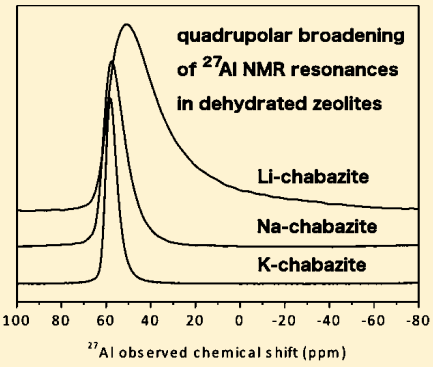

1. INTRODUCTION

Zeolites are crystalline microporous alumosilicates industrially employed as catalysts and sorbents. Their three-dimensional frameworks are made of corner-sharing SiO_4 and AlO_4^- tetrahedra. The isomorphous substitutions of Al atoms into the silicate framework result in the introduction of negative charges of AlO_4^- tetrahedra that are balanced by either protons or extraframework cationic species (metal cations and metal-oxo cations) which correspond to catalytic and sorption centers. Unique properties of the cationic species together with the variability of microporous channel systems of zeolites are responsible for the fact that zeolites represent a wide and very important group of heterogeneous catalysts.[1]

Because the extraframework species balance the negative charges of AlO_4^- tetrahedra, their properties are inseparably connected with the Al siting (i.e., which different distinguishable framework T sites are occupied by isolated Al atoms[2]) and Al distribution (i.e., distribution of the framework Al atoms between Al−O−Si−O−Si−O−Al sequences in the rings forming cationic sites for divalent cations and isolated Al atoms[2]) in the zeolite framework. These two properties govern the local structures of the active sites and their positions[3] in the zeolite channel system, which are key factors affecting the catalytic performance (i.e., activity, selectivity, and stability) of zeolite catalysts.[1] Therefore, the knowledge of the local structure of active sites and their locations in the zeolite channel system is essential for understanding the catalytic properties of zeolites and developing highly active, selective, and durable zeolite catalysts.

Diffraction methods are of limited use in analyzing extraframework cationic species in silicon-rich zeolites because of (i) their large unit cell, (ii) a medium or high number of crystallographically distinguishable framework T sites of which only some are partly occupied by Al atoms (i.e., Al(T)), (iii) more possible extraframework cationic sites for individual Al(T),[4] and (iv) low number of Al atoms in the framework (Si/Al > 8).[5] Therefore, the knowledge regarding the siting of cations and the local structure of cationic sites in silicon-rich zeolites is very limited.

The siting of monovalent cations exchanged in zeolites of the FER (K^+)[6] and MFI (Li^+,[7] Na^+,[7] K^+,[7] Rb^+,[7] Cu^+[8]) structures was investigated by diffraction methods, but a majority of

Received: April 30, 2016
Revised: June 8, 2016
Published: June 10, 2016

DOI: 10.1021/acs.jpcc.6b04391
J. Phys. Chem. C 2016, 120, 14216−14225

studies dealt with heavy ions (Cs^{+}[9−11] and Tl^{+}[7,12]) not very attractive for catalysis. Similarly, the siting of divalent cations was studied by X-ray diffraction for the zeolite of the FER structure with the Si/Al ratio of 8.5 (Co^{2+}[13] and Ni^{2+}[14]) and MOR[15] structure. Moreover, diffraction experiments provide only the positions of cations in the framework but not the local structure of the cationic sites as the coordinates of the cations are combined with the averaged coordinates of the framework reflecting mainly empty cationic sites and also the corresponding siliceous structures (i.e., without the framework Al/Si substitutions).

Diffraction techniques cannot distinguish between Al and Si atoms and thus do not allow direct identification of the Al siting in zeolites. Conversely, high-resolution ^{27}Al solid state NMR spectroscopy and applications of multiple-quantum methods and ultrahigh field magnets led to the recent success in determining the Al siting in the zeolites of the FER,[16] *BEA,[17] TON,[18] and MFI[19,20] (partial determination) structures. Tetrahedral framework Al atoms are in this case characterized by the nuclear quadrupolar coupling product, P_Q, around 2.5 MHz resulting in narrow ^{27}Al NMR signals.[21,22] Conversely, the nuclear quadrupolar coupling product P_Q of aluminum species in dehydrated zeolites ranges from 5 to 16 MHz, causing a marked broadening of the corresponding NMR signals.[23−25] In addition, the acquisition time of the corresponding ^{27}Al magic-angle spinning (MAS) NMR spectra substantially increases, and often the ^{27}Al NMR signal becomes "NMR invisible". The ^{27}Al MAS NMR experiments[16,17,19,20,26,27] on hydrated zeolites allowed only a determination of the siting of Al atoms in the T sites, but the local arrangement of the whole cationic site (i.e., the extraframework cation and the framework atoms forming the structure of the cationic site including the balanced framework Al atoms) could not have been analyzed. Only a few studies investigated dehydrated zeolites by ^{27}Al MAS NMR spectroscopy; therefore, our knowledge in this area is significantly limited.[23−25,28,29]

Freude and Hunger with collaborators demonstrated that it was possible to monitor Al atoms in dehydrated zeolites by ^{27}Al MAS NMR spectroscopy, and their results showed a variability of the ^{27}Al MAS NMR spectra and line widths for faujasite and ZSM-5 structures exchanged with Na and H cations.[23−25,28] Thus, the ^{27}Al MAS NMR spectra of dehydrated zeolites have to contain complex and detailed information (i) regarding the Al siting in the framework and (ii) concerning the local structure of the sites accommodating the extraframework cations in a dehydrated zeolite. However, this information has not been utilized yet. This is caused by the absence of understanding the mechanism of the broadening of the spectra and of the parameters controlling their width and shape. There is only a generally accepted hypothesis that narrow ^{27}Al NMR resonances of framework Al atoms in hydrated zeolites are caused by narrowing the broad ^{27}Al NMR resonances (due to the quadrupolar broadening) by averaging the electrostatic field around AlO_4^- tetrahedra due to molecular motion of water molecules.

In this article, we use high-resolution ^{27}Al MAS NMR spectroscopy of dehydrated Li-, Na-, and K- forms of chabazite (i.e., Li-CHA, Na-CHA, and K-CHA, respectively) in tandem with density functional theory (DFT) calculations to (i) investigate the quadrupolar interaction of ^{27}Al nuclei in dehydrated zeolites, (ii) understand high-resolution ^{27}Al MAS NMR spectra, and (iii) infer the local structure of the sites accommodating the extraframework M^+ cations.

2. EXPERIMENTAL SECTION

2.1. Preparation of the Samples. The parent CHA material (Si/Al 2.2) was prepared according to the procedure described in our prior study.[30] Zeolite Y (Si/Al 2.7) in ammonium form was used as a source material and was mixed with a solution of potassium hydroxide. The batch composition was $0.17Na_2O{:}2.0K_2O{:}Al_2O_3{:}5.4SiO_2{:}224H_2O$. The synthesis took place in a polypropylene bottle with a screw-top lid at a temperature of 640 °C for 96 h without agitation. After that, the product was recovered by filtration, washed repeatedly with deionized water, and dried at ambient temperature. X-ray diffraction and scanning electron microscopy confirmed a high crystallinity and phase purity of the parent sample, and ^{29}Si and ^{27}Al MAS NMR experiments verified the exclusive presence of tetrahedral Al atoms in the framework. The chemical composition was determined by X-ray fluorescence. The parent Na,K-CHA sample was ion-exchanged with 0.5 M NH_4NO_3 twice for 24 h to obtain the NH_4-form. Then the NH_4-CHA zeolite was exchanged into the M-CHA (M = Li, Na, and K) forms by repeated (3× 24 h) M^+ ion-exchange using 0.5 M MNO_3 (50 mL per 1 g of a zeolite) at 70 °C for Li^+ and ambient temperature for Na^+ and K^+. The three M-CHA samples were thoroughly washed with distilled water and then equilibrated on air at ambient temperature to guarantee their full hydration. The dehydrated M-CHA samples were obtained by in situ dehydration at 450 °C under dynamic vacuum (p = 0.2 Pa) for 4 h.

2.2. ^{27}Al MAS NMR Spectroscopy. Solid-state NMR spectra were measured at 11.7 T on a Bruker Avance III HD 500 WB/US NMR spectrometer with double-resonance 4 mm (for the hydrated samples) and 3.2 mm (for the dehydrated samples) probe heads. ^{27}Al MAS NMR single-pulse spectra were recorded using a single-pulse experiment with a $\pi/6$ (0.8 μs) excitation pulse and a 2 s repetition delay at the spinning frequency of 12 kHz and 20 kHz for the hydrated and dehydrated samples, respectively. Dipolar decoupling was applied during the data acquisition. The chemical shifts were referenced to the aqueous solution of $Al(NO_3)_3$. A low-temperature experiment with the K-CHA sample was performed at −80 °C employing an attached external cooling unit.

The two-dimensional (2D) triple-quantum ^{27}Al 3Q MAS NMR spectra of the dehydrated M-CHA samples were recorded using a three-pulse sequence with excitation, reconversion, and selective pulse lengths of 4.2, 1.5, and 43 μs, respectively. The reconversion and selective pulses were spaced using a z-filter of 20 μs in length. The spinning frequency was 20 kHz.

All spectra were analyzed using the DmFit software[31] to identify the individual ^{27}Al NMR resonances and their ^{27}Al NMR parameters.

3. COMPUTATIONAL MODELS AND METHODS

3.1. Computational Models. The starting structure of the chabazite framework is generated from the X-ray structure of chabazite.[32] All the computational models possess $P1$ symmetry.

3.1.1. Cationic Sites. Six models featuring one Al/Si substitution in the framework of the chabazite structure and

DOI: 10.1021/acs.jpcc.6b04391
J. Phys. Chem. C 2016, 120, 14216−14225

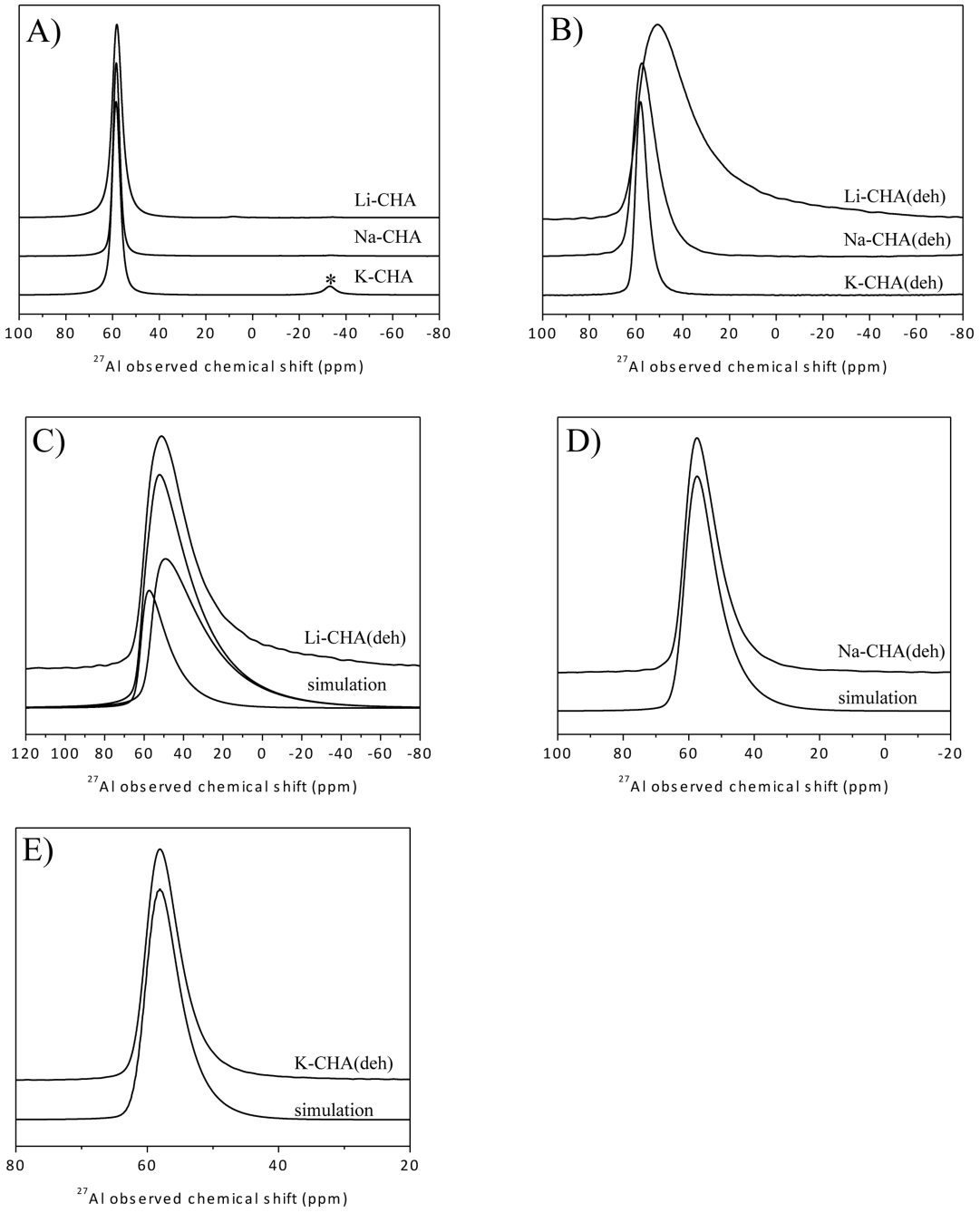

Figure 1. ^{27}Al MAS NMR spectra of the hydrated (A) and dehydrated (B) Li-CHA, Na-CHA, and K-CHA samples; ^{27}Al MAS NMR spectra and their simulations of the dehydrated Li-CHA (C; simulated using two resonances), Na-CHA (D; simulated using one resonance), and K-CHA (E; simulated using one resonance) samples. The asterisk (*) denotes a spinning sideband.

one M^+ (M^+ = Li^+, Na^+, and K^+) cation compensating the corresponding negative charge of AlO_4^- are employed. Three of the models, designated as Li^+-6-ring, Na^+-6-ring, and K^+-6-ring, feature the Li^+, Na^+, and K^+ cations, respectively, accommodated in the 6-ring while the other three, designated as Li^+-8-ring, Na^+-8-ring, and K^+-8-ring, respectively, are located in the 8-ring.

3.1.2. Bare Zeolite Framework Model. The model includes neither cations nor water molecules, features one Al/Si substitution, and bears a formal charge of −1.[18−20,26,27] It is adopted to calculate the local structure around the AlO_4^- tetrahedra and to predict the ^{27}Al NMR parameters in fully hydrated, cation-containing silicon-rich zeolites. The comparison between the results of this model and the models of the cationic sites (section 3.1.1.) allows the investigation of the effect of the change of the local structure of AlO_4^- (i.e., deformation) caused by the binding of M^+ to the zeolite framework on the ^{27}Al NMR parameters.

3.2. QM-Pot Method and Programs Used. The QM-Pot method employed[33,34] partitions of the whole system (S) into two parts. The inner part (I) is treated by QM, and the outer part (O) as well as all of the interactions between the inner and the outer layers are treated by parametrized Pot. The dangling bonds of the inner part are saturated by link hydrogen atoms. The atoms of the inner part together with the link atoms form the cluster (C). The QM-Pot approach is discussed in detail

DOI: 10.1021/acs.jpcc.6b04391
J. Phys. Chem. C 2016, 120, 14216−14225

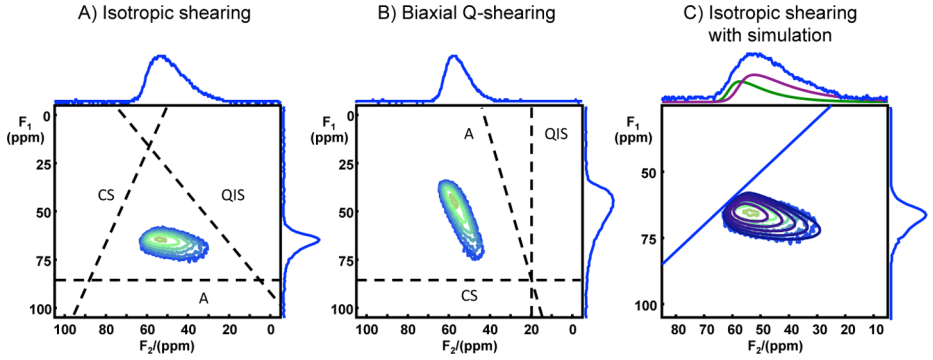

Figure 2. ^{27}Al 3Q MAS NMR spectra of the dehydrated Li-CHA sample: (A) isotropic shearing, (B) biaxial Q-shearing, and (C) isotropic shearing with simulation. The axes of the NMR contributions are shown as dashed lines marked as CS, QIS, and A.

elsewhere.[35] The calculations were performed by the QMPOT program,[34] which utilizes the Turbomole program[36−40] for the QM part and the GULP program[41,42] for the periodic potential function calculations. The hybrid DFT method, employing the B3LYP[43,44] functional and the TZVP basis set of Ahlrichs and co-workers,[45] was used for the QM calculations. Shell-model ion-pair potentials[46] parametrized on DFT results for zeolites[47] were employed as Pot. The electrostatic energy was evaluated by standard Ewald summation techniques for all cores and shells. A cutoff radius of 10 Å was chosen for the summation of short-range interactions. Our prior studies of the chabazite,[27] TON,[18] and MFI[19,20,26] structures using the QM-Pot method yielded ^{27}Al isotropic chemical shifts which were in very good agreement with the corresponding experimental values.

3.3. Optimization of Structures. Both the lattice constants and the atomic positions of the all-silica CHA structure were optimized by the GULP program at constant pressure. Then, one silicon atom was replaced by an aluminum atom compensated by M^+ (no cation was employed for the bare zeolite framework model, see section 3.1.2), and the structure and the lattice constants were further optimized at constant pressure. The optimized structures were subsequently used for defining a cluster around the Al atom for our QM-Pot calculations. The clusters were embedded, and the structure of the entire system was optimized by QMPOT at constant volume.

3.4. Cluster Models. Clusters having the Al atoms in the center and including five coordination shells (Al−O−Si−O−Si−O−H_{link}) and the M^+ cation (no cation was employed for the bare zeolite framework model, see section 3.1.2.) were used to calculate the structure of the cationic sites.[16,18−20,26,27,48] Because of the presence of silicate rings in the framework of CHA, the created clusters contained pairs of very close H_{link} atoms. Because the close H_{link} atoms represented the same Si atom, they were replaced by the corresponding $Si(OH_{link})_2$ moiety. This was repeated until the cluster contained no such pairs.

3.5. Calculations of ^{27}Al NMR Parameters. Subsequent to the QM-Pot structure determination, the Gaussian09 program[49] was employed to calculate ^{27}Al NMR shielding tensors; nuclear quadrupolar coupling constants,[50] C_Q; and asymmetry parameters,[50] η, for the ^{27}Al atom by the gauge independent atomic orbital method (GIAO)[51] using the B3LYP functional[43,44] and the pcS basis sets of Jensen:[52] pcS-4 for the Al and M atoms; pcS-1 for all the other atoms. The EFGShield program[50] was employed to extract the C_Q and η values from the Gaussian output files. Moreover, the nuclear quadrupolar coupling product P_Q, which is defined[53] as follows: $P_Q = C_Q(1 + \eta^2/3)^{1/2}$, was calculated from the C_Q and η values. These P_Q values can be compared with those obtained from simulations of the measured ^{27}Al MAS NMR spectra (section 4).

3.6. Calculations of the Contributions to the Effect of M^+ on the ^{27}Al NMR Parameters. To investigate the influence of the change of the local structure of AlO_4^- caused by the binding of M^+ to the zeolite framework without including the effect of the M^+ cation, the ^{27}Al NMR parameters were calculated (single-point computations) for the optimized structures (optimized with M^+) of the six models of the cationic sites with the removed M^+ cations (the models possess a formal charge of −1).

In addition, the optimized bare framework models with the added M^+ cations located in the same positions as in the corresponding cationic sites were used to calculate (single-point computations) the effect of the M^+ cations on the ^{27}Al NMR parameters with the exclusion of the influence of the change of the local structure of AlO_4^- (i.e., deformation) due to the coordination of M^+ to the zeolite framework. Furthermore, these calculations of the ^{27}Al NMR parameters were repeated and the M^+ cations were replaced by the background charge[54,55] of +1 located at the positions of M^+. These computations allow the evaluation of the effect of the +1 charge of the M^+ cation without including the other effects of the M^+ cation.

4. EXPERIMENTAL RESULTS

Figure 1 compares the single-pulse ^{27}Al MAS NMR spectra of the hydrated as well as dehydrated M-CHA (M = Li, Na, and K) samples and the deconvolution of the spectra of the dehydrated samples.

The dehydration of the samples is connected with a marked broadening of the ^{27}Al NMR signal. Moreover, this broadening depends on the cation balancing the framework negative charge.

^{27}Al 3Q MAS NMR spectra of the dehydrated M-CHA samples were collected to investigate the mechanism of line broadening in dehydrated zeolites. Note that the collection of the ^{27}Al MQ MAS NMR spectrum of an enormously broad signal requires the acquisition time of several days. Figure 2 shows the ^{27}Al 3Q MAS NMR spectrum and its simulation of the dehydrated Li-CHA sample.

Besides typical isotropic shearing transformation of ^{27}Al 3Q MAS NMR spectra, the biaxial Q-shearing of the 2D plot of the ^{27}Al 3Q MAS NMR spectra was applied (Figure 2) to elucidate

DOI: 10.1021/acs.jpcc.6b04391
J. Phys. Chem. C 2016, 120, 14216−14225

the mechanism of the ^{27}Al NMR signal broadening. The biaxial Q-shearing transformation completely removes the isotropic chemical shift from the indirect dimension in contrast to the isotropic shearing which minimizes the anisotropy contribution from the obtained 2D ^{27}Al 3Q MAS NMR spectrum. Thus, the spectrum purely reflects the second-order quadrupolar broadening and the quadrupole-induced shift.[56,57] The results shown in Figure 2B thus clearly evidence that the quadrupolar effect predominate in the broadening of the ^{27}Al (3Q) MAS NMR spectra of the dehydrated Li-CHA, Na-CHA, and K-CHA samples.

Both the single-pulse ^{27}Al MAS NMR and isotropically sheared ^{27}Al 3Q MAS NMR spectra of all the dehydrated samples were simultaneously fitted in the DmFit software using the "Czjzek simple" model to obtain the ^{27}Al NMR parameters. This function takes into account a Gaussian distribution of both of the isotropic chemical shifts and the distribution of quadrupolar couplings.[58] The spectra of the dehydrated Na-CHA and K-CHA samples were simulated using one resonance (Figure 1D,E) while two resonances (Figure 1C) were required for the dehydrated Li-CHA sample. The values of the ^{27}Al isotropic chemical shift and the nuclear quadrupolar coupling product P_Q[53] from the spectra simulations are shown in Table 1.

Table 1. Values of the ^{27}Al Isotropic Chemical Shift, δ_{iso}, and the Nuclear Quadrupolar Coupling Product, P_Q, from Simulations of the ^{27}Al MAS NMR Spectra of the Dehydrated and Hydrated M-CHA samples

	δ_{iso} (ppm)	P_Q (MHz)
dehydrated Li-CHA	62[a]	5.3
dehydrated Li-CHA	57[b]	7.3
dehydrated Na-CHA	61	4.2
dehydrated K-CHA	60	2.9
hydrated Li-CHA	60.0	2.4
hydrated Na-CHA	59.5	1.8
hydrated K-CHA	59.5	1.8
hydrated K-CHA at 190 K	59.7	2.1

[a]Resonance I. [b]Resonance II.

The effect of low temperature on the ^{27}Al MAS NMR spectrum of chabazite is revealed in Figure 3, which compares the ^{27}Al MAS NMR spectra of the hydrated K-CHA sample measured at −80 °C and at room temperature (RT).

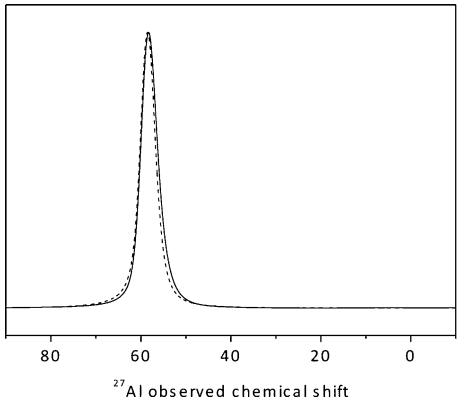

Figure 3. Effect of low temperature on the ^{27}Al MAS NMR spectrum of K-CHA. The spectra were recorded at −80 °C (—) and RT (- - -).

The decrease of the temperature is followed by only a negligible broadening of the spectrum; see also Table 1 which shows the ^{27}Al NMR parameters of the spectra.

5. COMPUTATIONAL RESULTS

Our calculations of the six models of the cationic sites yielded the optimized structures and the corresponding relative energies of the two cationic sites (M^+ accommodated in 6- and 8-rings), see Figure 4.

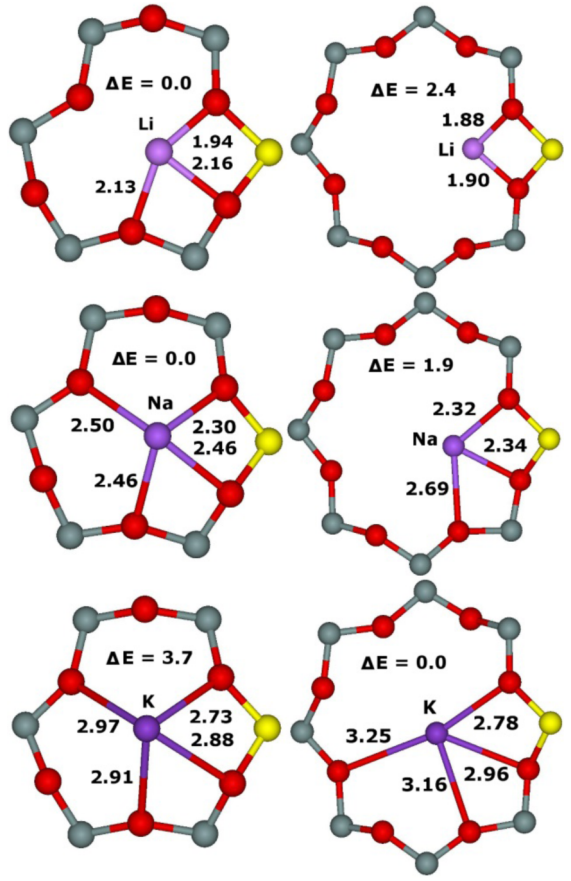

Figure 4. Optimized structures (M−O distances in angstroms) of the cationic sites of Li^+, Na^+, and K^+ accommodated in the 6- and 8-rings and the relative energies for each M^+ in kilocalories per mole. Silicon atoms are in gray, oxygen atoms in red, and aluminum atoms in yellow.

Our computational results show that all three M^+ cations are coordinated to two O atoms of AlO_4^- tetrahedra for both the sites. In addition, there is additional coordination to O atoms of SiO_4: one for Li^+-6-ring and Na^+-8-ring; two for Na^+-6-ring, K^+-6-ring, and K^+-8-ring. The smaller Li^+ and Na^+ cations accommodated in the 6-ring are calculated to be more stable by 2 kcal/mol, while the largest K^+ cation prefers the 8-ring by 4 kcal/mol.

Table 2 reveals the ^{27}Al NMR shielding values and the C_Q, η, and P_Q values for the Al atom. The ^{27}Al NMR parameters were also computed for the Al atom of the optimized bare zeolite framework model (Table 2).

The two distinct cationic sites differed in the ^{27}Al NMR shielding by 4 ppm for Li^+, 3 ppm for Na^+, and 1 ppm for K^+. The nuclear quadrupolar coupling constants C_Q of the ^{27}Al atom were the largest for the smallest cation Li^+, while they were smaller for the two larger cations. For Na^+ and K^+, the C_Q

DOI: 10.1021/acs.jpcc.6b04391
J. Phys. Chem. C 2016, 120, 14216−14225

Table 2. Relative Energies of the M^+ Sites and the ^{27}Al NMR Parameters (Shielding, C_Q, η, and P_Q) Calculated for the Computational Models[a]

		optimized cationic site							
		with M^{+}				removed M^{+}			
cation model	ΔE (kcal/mol)	shielding (ppm)	C_Q (MHz)	η	P_Q (MHz)	shielding (ppm)	C_Q (MHz)	η	P_Q (MHz)
Li^+-8-ring	2.4	505.2	9.3	0.28	9.4	505.8	6.8	0.22	6.9
Li^+-6-ring	0.0	509.4	9.5	0.77	10.4	509.5	7.2	0.74	7.8
Na^+-8-ring	1.9	505.8	5.9	0.58	6.2	506.7	4.0	0.86	4.5
Na^+-6-ring	0.0	508.9	7.5	0.98	8.6	509.5	5.6	0.98	6.4
K^+-8-ring	0.0	507.5	4.0	0.73	4.3	507.9	3.0	0.95	3.4
K^+-6-ring	3.7	508.9	6.2	0.91	7.0	509.2	4.7	0.85	5.2
		bare framework							
		with M^+				M^+ replaced by charge[b]			
		shielding (ppm)	C_Q (MHz)	η	P_Q (MHz)	shielding (ppm)	C_Q (MHz)	η	P_Q (MHz)
Li^+-8-ring		506.0	1.8	0.99	2.1	510.2	3.0	0.91	3.4
Li^+-6-ring		507.5	4.7	0.81	5.2	510.0	3.2	0.71	3.5
Na^+-8-ring		507.2	2.0	0.75	2.2	510.2	3.0	0.92	3.4
Na^+-6-ring		508.1	4.4	0.88	4.9	510.0	3.1	0.70	3.3
K^+-8-ring		508.8	2.3	0.78	2.5	510.2	3.0	0.89	3.4
K^+-6-ring		508.7	4.0	0.94	4.6	510.1	3.0	0.68	3.2

[a]The NMR parameters calculated for the bare framework model (section 3.1.2): shielding = 510.2 ppm, C_Q = 3.5 MHz, η = 0.83, P_q = 3.9 MHz. [b]Background charge at the positions of M^+.

values differed for the 8-ring (smaller) and 6-ring (larger) sites, while the values were almost the same for the two Li^+ sites. The asymmetry parameters, η, were systematically smaller for the 8-ring sites. The calculations of the NMR parameters for the optimized cationic sites with the removed M^+ cations (without any reoptimization of the structure) yielded the C_Q values which were smaller by ca. 2.4, 1.9, and 1.3 MHz for Li^+, Na^+, and K^+ cations, respectively. The values of η parameters are mainly only slightly changed.

The C_Q parameters computed for the optimized bare framework model with the added M^+ cations located in the same positions as in the corresponding cationic sites were significantly lower than those calculated for the optimized cationic sites (including M^+) by 7.5, 3.9, and 1.7 MHz for Li^+, Na^+, and K^+ located in the 8-ring, respectively, and by 4.8, 3.1, and 2.2 MHz for Li^+, Na^+, and K^+ occupying the 6-ring, respectively. It should be noted that the calculated C_Q values for all three M^+ cations present in the 8-ring were smaller than the corresponding values computed for the bare framework model without any cation (Table 2). In addition, when the M^+ cations were replaced by the background charge of +1 located at the positions of M^+, the calculated C_Q parameters were very uniform (3.0−3.2 MHz) for all three cations and both cationic sites (Table 2). These C_Q values were very close to that calculated for the bare framework model without any cation (Table 2).

6. DISCUSSION

6.1. Broadening of ^{27}Al NMR Signal of the Dehydrated Cationic Forms of Chabazite. Figure 1 shows the well-known enormous broadening of the ^{27}Al NMR resonances for the dehydrated samples. The ^{27}Al MAS NMR spectra of the dehydrated M-CHA (M = Li, Na, and K) zeolites significantly differ in their width depending on the cation balancing the negative charge of the AlO_4^- tetrahedra, although there is only one crystallographically distinguishable framework T site which could be occupied by Al atoms.[32] The largest broadening (i.e., the largest P_Q values of 5.3 and 7.3 MHz) is observed for the smallest cation Li^+, while the smallest broadening (i.e., the smallest P_Q value of 2.9 MHz) is observed for the largest cation K^+. The broadening for the Na-CHA sample (i.e., the P_Q value of 4.2 MHz) is between those for the Li-CHA and K-CHA materials. These results indicate (i) a significant role of the cation interaction with the zeolite framework in the broadening of the ^{27}Al MAS NMR signal upon dehydration of the M-CHA samples and (ii) a limited or negligible role of the motion of water molecules in zeolite channels causing "averaging" of the local electrostatic field and thus narrowing the ^{27}Al NMR resonances in hydrated zeolites. If the motion of water molecules was responsible for the narrow ^{27}Al NMR resonances in the hydrated zeolites, then the broadening upon dehydration would not depend on the cationic form.

6.1.1. Hydrated M-CHA Samples. The X-ray diffraction experiment for chabazite[32] showed one crystallographically distinguishable T site which can be occupied by Al atoms. Conversely, our combined ^{27}Al (3Q) MAS NMR and DFT study[27] allowed the identification of three Al(T) sites (i.e., Al/Si framework substitutions cause that one distinguishable framework T1 site to split into three subsets of the T1 site) with very close ^{27}Al isotropic chemical shifts (difference of 0.8 ppm) in the hydrated SSZ-13 zeolite (Si/Al 38) of the chabazite structure. Therefore, even if the splitting of the ^{27}Al NMR signal observed for the silicon-rich SSZ-13 zeolite occurs also for the aluminum-rich chabazite, we assume that these very close ^{27}Al NMR resonances would overlap with the broadening of ^{27}Al NMR resonances originating from the variability of middle-range and long-range orderings of the zeolite framework due to isomorphous substitutions of Al into the zeolite framework.[59] The observed ^{27}Al NMR signal therefore represents a Gaussian envelope of a number of close ^{27}Al NMR resonances. Thus, within the accuracy acceptable for this study, the ^{27}Al NMR signal of the hydrated M-CHA samples can be simulated using one resonance.

6.1.2. Dehydrated M-CHA Samples. Simulations of the single-pulse ^{27}Al MAS NMR spectra of the dehydrated M-CHA zeolites (Figure 1C−E) reveal one ^{27}Al NMR resonance for

DOI: 10.1021/acs.jpcc.6b04391
J. Phys. Chem. C 2016, 120, 14216−14225

Na^+ and K^+ and two ^{27}Al NMR resonances for Li^+ that are subsequently confirmed by our ^{27}Al 3Q MAS NMR experiments (Figure 2). Two main cationic sites occupied by Na^+ in dehydrated Na-CHA[60] were reported. A possibility that two distinct M^+ sites corresponding to the same Al(T) atom could be occupied concurrently was shown by ^7Li MAS NMR experiments combined with DFT experiments.[4] The presence of two types of ^{27}Al atoms with significantly different NMR parameters, which moreover depend on the cation type, can be therefore attributed to the effect of two occupied cationic sites corresponding to the same Al(T).

Tables 1 and 2 show that the measured and calculated, respectively, ^{27}Al NMR parameters of the three dehydrated zeolites are in good agreement, indicating that both the computational model and the theoretical approach provide realistic results regarding (i) the structure of the cationic sites including the local structure of the AlO_4^- tetrahedra and (ii) the ^{27}Al NMR parameters. The agreement reveals that the significant increase of the quadrupolar interaction, which is the most remarkable feature of the ^{27}Al MAS NMR spectra of dehydrated zeolites, of the ^{27}Al NMR resonances in the dehydrated zeolites occurs because of the strong coordination of the extraframework M^+ cation in the vicinity of the framework Al atom. Note that the calculations were performed for the silicon-rich chabazite SSZ-13 with one isolated Al atom per unit cell (Si/Al 35) while the ^{27}Al (3Q) MAS NMR spectra were recorded for the aluminum-rich material (Si/Al 2.2) containing many Al−O−Si−O−Al sequences in the zeolite framework[59] and having majority of 6- and 8-rings occupied by extraframework M^+ cations.

The effect of the binding of M^+ to the zeolite framework upon dehydration on the ^{27}Al NMR parameters is composed of two contributions (sections 3.6 and 5): (i) the change of the local structure of AlO_4^- (i.e., deformation) caused by the binding of M^+ to the zeolite framework without including the effect of the M^+ cation and (ii) the effect of the M^+ cation with the exclusion of the influence of the change of the local structure of AlO_4^- due to the coordination of M^+ to the zeolite framework. The latter could be further investigated employing the background (point) +1 charge instead of the M^+ cation. These calculations (sections 3.6 and 5) permit the evaluation of the effect of the +1 charge of the cation M^+ without including the other effects of the cation M^+.

The calculations of the ^{27}Al NMR parameters for the optimized cationic sites with the removed M^+ cations (Table 2) reveal that the main factor responsible for the enormous broadening of the ^{27}Al NMR resonances of the dehydrated samples is the deformation of the local structure of AlO_4^- due to the binding of M^+ to the zeolite framework. The calculated P_Q values were only slightly smaller by ca. 2.6, 2.0, and 1.4 MHz for Li^+, Na^+, and K^+ cations, respectively, than those calculated with the presence of the M^+ cations (Table 2 and Figure 5).

Conversely, the influence of M^+, without considering the deformation of the local structure of AlO_4^- due to the binding of M^+ to the zeolite framework, is significantly smaller. The calculated P_Q values for the optimized bare framework model with the added M^+ cations located in the same positions as in the corresponding cationic sites are significantly smaller (Table 2 and Figure 5). They are close to the P_Q value computed for the bare zeolite framework model with no cation (i.e., 3.9 MHz; see Table 2). The P_Q values calculated for M^+ accommodated in the 6-ring are slightly larger than 3.9 MHz, while those computed for M^+ located in the 8-ring are slightly smaller. This

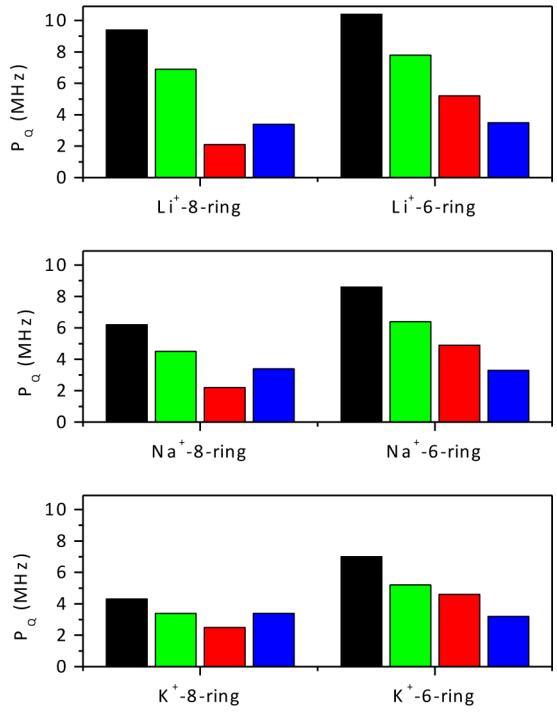

Figure 5. Calculated P_Q values for (i) the Li^+-8-ring, Li^+-6-ring, Na^+-8-ring, Na^+-6-ring, K^+-8-ring, and K^+-6-ring models (black bars); (ii) the six models with the removed M^+ (green bars); (iii) the bare framework model with the added M^+ cations (red bars); and (iv) the bare framework model with the added +1 background charges (blue bars).

indicates that the effect of the M^+ cation on the P_Q parameters with the exclusion of the influence of the deformation of the local structure of AlO_4^- can both increase as well as decrease, depending on the M^+ position with respect to AlO_4^-, the values of the P_Q parameter of the ^{27}Al atom of the AlO_4^- tetrahedron which is compensated by the M^+ cation. In addition, our calculations employing the background charge of +1 located at the positions of M^+ reveal a negligible effect of the +1 charge as the calculated P_Q parameters for all the six models (Table 2) are very close to the P_Q calculated for the bare framework model without any cation. Our results indicate that the four O atoms of the $^{27}AlO_4^-$ tetrahedron shield the ^{27}Al atom and thus minimize the effect of the charge of the cation balancing the negative charge of AlO_4^-. The quadrupolar interaction decreases with the increasing diameter of the monovalent cation balancing the Al atom as the local deformation of the cationic site in the zeolite is less pronounced when accommodating a larger cation.

Although this study deals with the Al-rich Li-, Na-, and K-forms of chabazite, its results can be generalized to other zeolites and cations. With the exception of Li^+, cationic sites in zeolites (including pentasil ones) are generally formed by 6- and 8-rings. Therefore, the deformation of the local structure of AlO_4^- due to the binding of M^+ to the zeolite framework should be similar for other zeolites. The mechanism of the broadening of the ^{27}Al NMR signal due to the strong coordination should be similar for all cations. However, the correlation between the cation size and the nuclear quadrupolar coupling product P_Q is less clear. The extrapolation of the effect of the cation size on the broadening of the ^{27}Al NMR signal cannot be made because the increase of the deformation of the

DOI: 10.1021/acs.jpcc.6b04391
J. Phys. Chem. C 2016, 120, 14216−14225

AlO_4^- tetrahedra by the coordination of extra-large cations to 8-rings cannot be excluded and requires further study.

6.2. Effect of Water on the ^{27}Al NMR Signal of the Cationic Forms of Chabazite. Our ^{27}Al MAS NMR experiments on the three dehydrated samples show that the broadening of the ^{27}Al NMR resonances depends on the type of the cation (Figure 1). This result suggests a limited or negligible role of water molecules in narrowing the ^{27}Al NMR resonances of the hydrated samples. To further investigate the role of the motion of water molecules on the ^{27}Al NMR parameters, the ^{27}Al MAS NMR spectrum of the hydrated K-CHA sample was measured at −80 °C. Figure 3 compares this spectrum with that observed at RT. There is only a tiny broadening of the spectrum recorded at −80 °C (the P_Q value increased from 1.8 to 2.1 MHz, see Table 1), indicating that averaging the local field in the hydrated zeolites by water motion is not responsible for the weak quadrupolar interaction and the narrow ^{27}Al MAS spectra of the hydrated samples.

The observed P_Q values for the three hydrated M-CHA samples (2.4 MHz (Li^+), 1.8 MHz (Na^+), 1.8 MHz (K^+), Table 1) are close to those calculated for the ^{27}Al atom using the bare framework model with no cation (3.9 MHz, Table 2). This agreement suggests that the electric field gradient at the framework ^{27}Al atom nucleus is given by the charge and the geometrical arrangements of the four O atoms of the AlO_4^- tetrahedron. The AlO_4^- tetrahedron of the bare framework model with no cation is highly symmetric; therefore, the electric field gradient at the framework ^{27}Al atom nucleus is small, resulting in a low P_Q value and a narrow and symmetric ^{27}Al NMR signal.

Several studies showed that cations in hydrated zeolites were solvated and located in the zeolite channels.[15,32,61−63] Therefore, the local structures of the AlO_4^- tetrahedra correspond to that of the bare framework model. This is the reason why, in contrast to other solid materials, framework Al atoms in hydrated zeolites exhibit narrow and Gaussian-like signals.[21,64,65] The essential role of water molecules in hydrated zeolite is to prevent a strong coordination of the cations to the framework oxygens. The cations in hydrated zeolites can be only weakly coordinated to oxygen atoms of AlO_4^- tetrahedra, but they are mobile and they cannot deform the local structure of AlO_4^- tetrahedra. This result also explains why the bare framework model with neither extraframework cations nor water molecules can be used for realistic predictions of the isotropic chemical shifts of ^{27}Al atoms in individual framework T sites allowing the analysis of the Al siting in silicon-rich zeolites.[4,16−20,27] The extraframework cations are coordinated to the framework oxygen atoms when the zeolites are dehydrated. The local structure and the partial charges of the atoms of the AlO_4^- tetrahedra are changed, the symmetry of AlO_4^- tetrahedron is perturbed, and a significant broadening of the ^{27}Al signal occurs. This is also followed by the change of the signal shape from Gaussian-like to that typical for the quadrupolar broadening.

6.3. Local Structure of Extraframework Cationic Sites in the Vicinity of Individual Framework Al Atoms and the Siting of Al Atoms in the Framework T Sites. Our results reveal that ^{27}Al MAS NMR spectroscopy of dehydrated zeolites in tandem with DFT calculations can provide information regarding the local structures of cationic site as well as concerning the siting of Al atoms in the framework T sites and the local structure of AlO_4^- tetrahedra. In addition, this combined experimental and theoretical approach can yield data concerning the local structure of cationic sites of cations that are NMR "invisible", as, for example, K^+ ions. Na-forms of dehydrated zeolites are suggested to be the most promising for analysis of the Al siting because Na^+ cations in contrast to Li^+ exhibit a lower number of possible cationic sites with respect to one Al(T) atom. Moreover, Na^+ cations in opposition to larger cations affect the local structure of AlO_4^- tetrahedra more significantly; therefore, the ^{27}Al NMR parameters should be more specific for the individual Al(T) sites as well as the types of the cationic sites. However, ^{27}Al MAS NMR of dehydrated zeolites can be applied for this purpose only for zeolites with a lower number of framework T sites because of the complexity of the ^{27}Al NMR spectra of dehydrated zeolites.

7. CONCLUSION

Al atoms in frameworks of hydrated zeolites exhibit a tetrahedral coordination that results in an extremely low quadrupolar broadening of the ^{27}Al NMR resonances. Extraframework cations balancing the negative charge of framework AlO_4^- tetrahedra are solvated and mobile and do not significantly perturb the structure of the AlO_4^- tetrahedra in hydrated zeolites. A dehydration of zeolites results in a coordination of extraframework cations to O atoms of the AlO_4^- and SiO_4 tetrahedra followed by their significant deformation leading to a perturbation of the symmetry of AlO_4^- tetrahedron and therefore significant broadening of the ^{27}Al NMR signal. The effect of the cation binding consists of two contributions: (i) the deformation of the local structure of AlO_4^- due to the binding of M^+ to the zeolite framework and (ii) the effect of the M^+ cation with the exclusion of the influence of the deformation of the local structure of AlO_4^-. Our results show that the former is responsible for the broadening of the ^{27}Al NMR signals. The quadrupolar interaction decreases with the increasing diameter of the monovalent cation balancing the AlO_4^- tetrahedron as the deformation is less pronounced for larger cations.

The influence of water in hydrated zeolites is limited only to the prevention of a strong coordination of the M^+ cation to O atoms of the AlO_4^- tetrahedra, but there is no "averaging" effect concerning the local electrostatic field due to molecular motion of water molecules. Our results show that the ^{27}Al NMR parameters in dehydrated zeolites can be calculated accurately enough to permit the description of the local structure of AlO_4^- tetrahedra in dehydrated zeolites. Moreover, the ^{27}Al NMR parameters can provide information regarding the cation siting in extraframework positions and the local structure of cationic sites.

AUTHOR INFORMATION

Corresponding Author

*E-mail: stepan.sklenak@jh-inst.cas.cz. Tel: (+420) 266 053 607.

Present Address

‖L.K.: University of Ottawa, Department of Chemistry and CCRI, 10 Marie Curie Pvt. D'Iorio Hall, Ottawa, Ontario K1N6N5, Canada.

Notes

The authors declare no competing financial interest.

ACKNOWLEDGMENTS

This work was supported by the by the Grant Agency of the Czech Republic (15-13876S and 15-14007S) and the RVO

DOI: 10.1021/acs.jpcc.6b04391
J. Phys. Chem. C 2016, 120, 14216−14225

(61388955). This work was supported by the IT4Innovations Centre of Excellence project (CZ.1.05/1.1.00/02.0070), funded by the European Regional Development Fund and the national budget of the Czech Republic via the Research and Development for Innovations Operational Programme, as well as Czech Ministry of Education, Youth and Sports via the project Large Research, Development and Innovations Infrastructures (LM2011033).

REFERENCES

(1) Dedecek, J.; Sobalik, Z.; Wichterlova, B. Siting and Distribution of Framework Aluminium Atoms in Silicon-Rich Zeolites and Impact on Catalysis. *Catal. Rev.: Sci. Eng.* **2012**, *54*, 135−223.

(2) Sklenak, S.; Andrikopoulos, P. C.; Whittleton, S. R.; Jirglova, H.; Sazama, P.; Benco, L.; Bucko, T.; Hafner, J.; Sobalik, Z. Effect of the Al Siting on the Structure of Co(II) and Cu(II) Cationic Sites in Ferrierite. A Periodic DFT Molecular Dynamics and FTIR Study. *J. Phys. Chem. C* **2013**, *117*, 3958−3968.

(3) Pashkova, V.; Sklenak, S.; Klein, P.; Urbanova, M.; Dedecek, J. Location of Framework Al Atoms in the Channels of ZSM-5: Effect of the (Hydrothermal) Synthesis. *Chem. - Eur. J.* **2016**, *22*, 3937−3941.

(4) Klein, P.; Dedecek, J.; Thomas, H. M.; Whittleton, S. R.; Pashkova, V.; Brus, J.; Kobera, L.; Sklenak, S. NMR Crystallography of Monovalent Cations in Inorganic Matrixes: Li^+ Siting and the Local Structure of Li^+ Sites in Ferrierites. *Chem. Commun.* **2015**, *51*, 8962−8965.

(5) Database of Zeolite Structures. http://www.iza-structure.org/databases.

(6) Pickering, I. J.; Maddox, P. J.; Thomas, J. M.; Cheetham, A. K. A Neutron Powder Diffraction Analysis of Potassium-Exchanged Ferrierite. *J. Catal.* **1989**, *119*, 261−265.

(7) Mentzen, B. F. Crystallographic Determination of the Positions of the Monovalent H, Li, Na, K, Rb, and Tl Cations in Fully Dehydrated MFI Type Zeolites. *J. Phys. Chem. C* **2007**, *111*, 18932−18941.

(8) Mentzen, B. F.; Bergeret, G. Crystallographic Determination of the Positions of the Copper Cations in Zeolite MFI. *J. Phys. Chem. C* **2007**, *111*, 12512−12516.

(9) Olson, D. H.; Khosrovani, N.; Peters, A. W.; Toby, B. H. Crystal Structure of Dehydrated CsZSM-5 (5.8Al): Evidence for Nonrandom Aluminum Distribution. *J. Phys. Chem. B* **2000**, *104*, 4844−4848.

(10) Mentzen, B. F.; Bergeret, G.; Emerich, H.; Weber, H. P. Dehydrated and Cs^+-Exchanged MFI Zeolites: Location and Population of Cs^+ from in Situ Diffraction Data as a Function of Temperature and Degree of Exchange. *J. Phys. Chem. B* **2006**, *110*, 97−106.

(11) Kim, C. W.; Heo, N. H.; Seff, K. Framework Sites Preferred by Aluminum in Zeolite ZSM-5. Structure of a Fully Dehydrated, Fully Cs^+-Exchanged ZSM-5 Crystal (MFI, Si/Al = 24). *J. Phys. Chem. C* **2011**, *115*, 24823−24838.

(12) Heo, N. H.; Kim, C. W.; Kwon, H. J.; Kim, G. H.; Kim, S. H.; Hong, S. B.; Seff, K. Detailed Determination of the Tl^+ Positions in Zeolite Tl-ZSM-5. Single-Crystal Structures of Fully Dehydrated Tl-ZSM-5 and H-ZSM-5 (MFI, Si/Al = 29). Additional Evidence for a Nonrandom Distribution of Framework Aluminum. *J. Phys. Chem. C* **2009**, *113*, 19937−19956.

(13) Dalconi, M. C.; Alberti, A.; Cruciani, G.; Ciambelli, P.; Fonda, E. Siting and Coordination of Cobalt in Ferrierite: XRD and EXAFS Studies at Different Co Loadings. *Microporous Mesoporous Mater.* **2003**, *62*, 191−200.

(14) Dalconi, M. C.; Cruciani, G.; Alberti, A.; Ciambelli, P.; Rapacciuolo, M. T. Ni^{2+} ion Sites in Hydrated and Dehydrated Forms of Ni-Exchanged Zeolite Ferrierite. *Microporous Mesoporous Mater.* **2000**, *39*, 423−430.

(15) Mortier, W. J. *Extraframework Cationic Positions in Zeolites*; Elsevier: Amsterdam, 1982.

(16) Dedecek, J.; Lucero, M. J.; Li, C.; Gao, F.; Klein, P.; Urbanova, M.; Tvaruzkova, Z.; Sazama, P.; Sklenak, S. Complex Analysis of the Aluminum Siting in the Framework of Silicon-Rich Zeolites. A Case Study on Ferrierites. *J. Phys. Chem. C* **2011**, *115*, 11056−11064.

(17) Vjunov, A.; Fulton, J. L.; Huthwelker, T.; Pin, S.; Mei, D.; Schenter, G. K.; Govind, N.; Camaioni, D. M.; Hu, J. Z.; Lercher, J. A. Quantitatively Probing the Al Distribution in Zeolites. *J. Am. Chem. Soc.* **2014**, *136*, 8296−8306.

(18) Sklenak, S.; Dedecek, J.; Li, C.; Gao, F.; Jansang, B.; Boekfa, B.; Wichterlova, B.; Sauer, J. Aluminum Siting in the ZSM-22 and Theta-1 Zeolites Revisited: A QM/MM Study. *Collect. Czech. Chem. Commun.* **2008**, *73*, 909−920.

(19) Sklenak, S.; Dedecek, J.; Li, C.; Wichterlova, B.; Gabova, V.; Sierka, M.; Sauer, J. Aluminum Siting in Silicon-Rich Zeolite Frameworks: A Combined High-Resolution ^{27}Al NMR Spectroscopy and Quantum Mechanics/Molecular Mechanics Study of ZSM-5. *Angew. Chem., Int. Ed.* **2007**, *46*, 7286−7289.

(20) Sklenak, S.; Dedecek, J.; Li, C.; Wichterlova, B.; Gabova, V.; Sierka, M.; Sauer, J. Aluminium Siting in the ZSM-5 Framework by Combination of High Resolution ^{27}Al NMR and DFT/MM Calculations. *Phys. Chem. Chem. Phys.* **2009**, *11*, 1237−1247.

(21) van Bokhoven, J. A.; Koningsberger, D. C.; Kunkeler, P.; van Bekkum, H.; Kentgens, A. P. M. Stepwise Dealumination of Zeolite Beta at Specific T-Sites Observed with ^{27}Al MAS and ^{27}Al MQ MAS NMR. *J. Am. Chem. Soc.* **2000**, *122*, 12842−12847.

(22) Kanellopoulos, J.; Unger, A.; Schwieger, W.; Freude, D. Catalytic and Multinuclear MAS NMR Studies of a Thermally Treated Zeolite ZSM-5. *J. Catal.* **2006**, *237*, 416−425.

(23) Freude, D.; Ernst, H.; Wolf, I. Solid-State Nuclear-Magnetic-Resonance Studies of Acid Sites in Zeolites. *Solid State Nucl. Magn. Reson.* **1994**, *3*, 271−286.

(24) Jiao, J.; Altwasser, S.; Wang, W.; Weitkamp, J.; Hunger, M. State of Aluminum in Dealuminated, Nonhydrated Zeolites Y Investigated by Multinuclear Solid-State NMR Spectroscopy. *J. Phys. Chem. B* **2004**, *108*, 14305−14310.

(25) Jiao, J.; Kanellopoulos, J.; Wang, W.; Ray, S. S.; Foerster, H.; Freude, D.; Hunger, M. Characterization of Framework and Extra-Framework Aluminum Species in Non-Hydrated Zeolites Y by ^{27}Al Spin-Echo, High-Speed MAS, and MQMAS NMR Spectroscopy at B_0 = 9.4 to 17.6 T. *Phys. Chem. Chem. Phys.* **2005**, *7*, 3221−3226.

(26) Dedecek, J.; Sklenak, S.; Li, C.; Wichterlova, B.; Gabova, V.; Brus, J.; Sierka, M.; Sauer, J. Effect of Al-Si-Al and Al-Si-Si-Al Pairs in the ZSM-5 Zeolite Framework on the ^{27}Al NMR Spectra. A Combined High-Resolution ^{27}Al NMR and DFT/MM Study. *J. Phys. Chem. C* **2009**, *113*, 1447−1458.

(27) Dedecek, J.; Sklenak, S.; Li, C.; Gao, F.; Brus, J.; Zhu, Q.; Tatsumi, T. Effect of Al/Si Substitutions and Silanol Nests on the Local Geometry of Si and Al Framework Sites in Silicone-Rich Zeolites: A Combined High Resolution ^{27}Al and ^{29}Si NMR and Density Functional Theory/Molecular Mechanics Study. *J. Phys. Chem. C* **2009**, *113*, 14454−14466.

(28) Ernst, H.; Freude, D.; Wolf, I. Multinuclear Solid-State NMR-Studies of Bronsted Sites in Zeolites. *Chem. Phys. Lett.* **1993**, *212*, 588−596.

(29) Brus, J.; Kobera, L.; Schoefberger, W.; Urbanova, M.; Klein, P.; Sazama, P.; Tabor, E.; Sklenak, S.; Fishchuk, A. V.; Dedecek, J. Structure of Framework Aluminum Lewis Sites and Perturbed Aluminum Atoms in Zeolites as Determined by $^{27}Al\{^1H\}$ REDOR (3Q) MAS NMR Spectroscopy and DFT/Molecular Mechanics. *Angew. Chem., Int. Ed.* **2015**, *54*, 541−545.

(30) Dedecek, J.; Wichterlova, B.; Kubat, P. Siting of the Cu^+ Ions in Dehydrated Ion Exchanged Synthetic and Natural Chabasites: A Cu^+ Photoluminescence Study. *Microporous Mesoporous Mater.* **1999**, *32*, 63−74.

(31) Massiot, D.; Fayon, F.; Capron, M.; King, I.; Le Calve, S.; Alonso, B.; Durand, J. O.; Bujoli, B.; Gan, Z. H.; Hoatson, G. Modelling One- and Two-Dimensional Solid-State NMR Spectra. *Magn. Reson. Chem.* **2002**, *40*, 70−76.

(32) Smith, J. V.; Glasser, L. S. D.; Rinaldi, F. Crystal Structures with a Chabazite Framework. II. Hydrated Ca-Chabazite at Room Temperature. *Acta Crystallogr.* **1963**, *16*, 45−53.

DOI: 10.1021/acs.jpcc.6b04391
J. Phys. Chem. C 2016, 120, 14216−14225

(33) Eichler, U.; Kolmel, C. M.; Sauer, J. Combining Ab Initio Techniques with Analytical Potential Functions for Structure Predictions of Large Systems: Method and Application to Crystalline Silica Polymorphs. *J. Comput. Chem.* **1997**, *18*, 463−477.
(34) Sierka, M.; Sauer, J. Finding Transition Structures in Extended Systems: A Strategy Based on a Combined Quantum Mechanics-Empirical Valence Bond Approach. *J. Chem. Phys.* **2000**, *112*, 6983−6996.
(35) Brandle, M.; Sauer, J. Acidity Differences between Inorganic Solids Induced by their Framework Structure. A Combined Quantum Mechanics Molecular Mechanics Ab Initio Study on Zeolites. *J. Am. Chem. Soc.* **1998**, *120*, 1556−1570.
(36) Haser, M.; Ahlrichs, R. Improvements on the Direct SCF Method. *J. Comput. Chem.* **1989**, *10*, 104−111.
(37) Eichkorn, K.; Treutler, O.; Ohm, H.; Haser, M.; Ahlrichs, R. Auxiliary Basis-Sets to Approximate Coulomb Potentials (Chem. Phys. Letters 240 (1995) 283−290). *Chem. Phys. Lett.* **1995**, *242*, 652−660.
(38) Eichkorn, K.; Treutler, O.; Ohm, H.; Haser, M.; Ahlrichs, R. Auxiliary Basis-Sets to Approximate Coulomb Potentials. *Chem. Phys. Lett.* **1995**, *240*, 283−290.
(39) Eichkorn, K.; Weigend, F.; Treutler, O.; Ahlrichs, R. Auxiliary Basis Sets for Main Row Atoms and Transition Metals and their Use to Approximate Coulomb Potentials. *Theor. Chem. Acc.* **1997**, *97*, 119−124.
(40) Treutler, O.; Ahlrichs, R. Efficient Molecular Numerical-Integration Schemes. *J. Chem. Phys.* **1995**, *102*, 346−354.
(41) Gale, J. D. GULP: A Computer Program for the Symmetry-Adapted Simulation of Solids. *J. Chem. Soc., Faraday Trans.* **1997**, *93*, 629−637.
(42) Gale, J. D.; Rohl, A. L. The General Utility Lattice Program (GULP). *Mol. Simul.* **2003**, *29*, 291−341.
(43) Lee, C. T.; Yang, W. T.; Parr, R. G. Development of the Colle-Salvetti Correlation-Energy Formula into a Functional of the Electron-Density. *Phys. Rev. B: Condens. Matter Mater. Phys.* **1988**, *37*, 785−789.
(44) Becke, A. D. Density-Functional Thermochemistry. III. The Role of Exact Exchange. *J. Chem. Phys.* **1993**, *98*, 5648−5652.
(45) Schafer, A.; Huber, C.; Ahlrichs, R. Fully Optimized Contracted Gaussian-Basis Sets of Triple Zeta Valence Quality for Atoms Li to Kr. *J. Chem. Phys.* **1994**, *100*, 5829−5835.
(46) Catlow, C. R. A.; Dixon, M.; Mackrodt, W. C. Inter-Ionic Potentials in Ionic Solids. *Lect. Notes Phys.* **1982**, *166*, 130−161.
(47) Sierka, M.; Sauer, J. Structure and Reactivity of Silica and Zeolite Catalysts by a Combined Quantum Mechanics Shell-Model Potential Approach Based on DFT. *Faraday Discuss.* **1997**, *106*, 41−62.
(48) Bussemer, B.; Schroder, K. P.; Sauer, J. Ab Initio Predictions of Zeolite Structures and ^{29}Si NMR Chemical Shifts. *Solid State Nucl. Magn. Reson.* **1997**, *9*, 155−164.
(49) Frisch, M. J., et al. *Gaussian 09*, revision C.01; Gaussian, Inc.: Wallingford, CT, 2011.
(50) Adiga, S.; Aebi, D.; Bryce, D. L. EFG Shield - A Program for Parsing and Summarizing the Results of Electric Field Gradient and Nuclear Magnetic Shielding Tensor Calculations. *Can. J. Chem.* **2007**, *85*, 496−505.
(51) Wolinski, K.; Hinton, J. F.; Pulay, P. Efficient Implementation of the Gauge-Independent Atomic Orbital Method for NMR Chemical-Shift Calculations. *J. Am. Chem. Soc.* **1990**, *112*, 8251−8260.
(52) Jensen, F. Basis Set Convergence of Nuclear Magnetic Shielding Constants Calculated by Density Functional Methods. *J. Chem. Theory Comput.* **2008**, *4*, 719−727.
(53) Baltisberger, J. H.; Xu, Z.; Stebbins, J. F.; Wang, S. H.; Pines, A. Triple-Quantum Two-Dimensional ^{27}Al Magic-Angle Spinning Nuclear Magnetic Resonance Spectroscopic Study of Aluminosilicate and Aluminate Crystals and Glasses. *J. Am. Chem. Soc.* **1996**, *118*, 7209−7214.
(54) Hall, G. G.; Smith, C. M. Fitting Electron-Densities of Molecules. *Int. J. Quantum Chem.* **1984**, *25*, 881−890.
(55) Smith, C. M.; Hall, G. G. The Approximation of Electron-Densities. *Theor. Chim. Acta* **1986**, *69*, 63−69.
(56) Kobera, L.; Brus, J.; Klein, P.; Dedecek, J.; Urbanova, M. Biaxial Q-Shearing of ^{27}Al 3QMAS NMR Spectra: Insight into the Structural Disorder of Framework Aluminosilicates. *Solid State Nucl. Magn. Reson.* **2014**, *57*−*58*, 29−38.
(57) Brus, J.; Kobera, L.; Urbanova, M.; Dousova, B.; Lhotka, M.; Kolousek, D.; Kotek, J.; Cuba, P.; Czernek, J.; Dedecek, J. Interface Induced Growth and Transformation of Polymer-Conjugated Proto-Crystalline Phases in Aluminosilicate Hybrids: A Multiple-Quantum ^{23}Na-^{23}Na MAS NMR Correlation Spectroscopy Study. *Langmuir* **2016**, *32*, 2787−2797.
(58) Neuville, D. R.; Cormier, L.; Massiot, D. Al Environment in Tectosilicate and Peraluminous Glasses: A ^{27}Al MQ-MAS NMR, Raman, and XANES Investigation. *Geochim. Cosmochim. Acta* **2004**, *68*, 5071−5079.
(59) Akporiaye, D. E.; Dahl, I. M.; Mostad, H. B.; Wendelbo, R. Aluminum Distribution in Chabazite: An Experimental and Computational Study. *J. Phys. Chem.* **1996**, *100*, 4148−4153.
(60) Mortier, W. J.; Pluth, J. J.; Smith, J. V. Positions of Cations and Molecules in Zeolites with Chabazite Framework. III. Dehydrated Na-Exchanged Chabazite. *Mater. Res. Bull.* **1977**, *12*, 241−249.
(61) Dedecek, J.; Wichterlova, B. Role of Hydrated Cu Ion Complexes and Aluminum Distribution in the Framework on the Cu Ion Siting in ZSM-5. *J. Phys. Chem. B* **1997**, *101*, 10233−10240.
(62) Dedecek, J.; Wichterlova, B. Co^{2+} Ion Siting in Pentasil-Containing Zeolites. I. Co^{2+} Ion Sites and their Occupation in Mordenite. A Vis-NIR Diffuse Reflectance Spectroscopy Study. *J. Phys. Chem. B* **1999**, *103*, 1462−1476.
(63) Chu, P. J.; Gerstein, B. C.; Nunan, J.; Klier, K. A Study of Solid-State NMR of ^{133}Cs and ^{1}H of a Hydrated and Dehydrated Cesium Mordenite. *J. Phys. Chem.* **1987**, *91*, 3588−3592.
(64) Sarv, P.; Fernandez, C.; Amoureux, J. P.; Keskinen, K. Distribution of Tetrahedral Aluminium Sites in ZSM-5 Type Zeolites: An ^{27}Al (Multiquantum) Magic Angle Spinning NMR Study. *J. Phys. Chem.* **1996**, *100*, 19223−19226.
(65) Kunkeler, P. J.; Zuurdeeg, B. J.; van der Waal, J. C.; van Bokhoven, J. A.; Koningsberger, D. C.; van Bekkum, H. Zeolite Beta: The Relationship between Calcination Procedure, Aluminum Configuration, and Lewis Acidity. *J. Catal.* **1998**, *180*, 234−244.

DOI: 10.1021/acs.jpcc.6b04391
J. Phys. Chem. C 2016, 120, 14216−14225